International Journal of Impact Engineering 38 (2011) 577–589

Contents lists available at ScienceDirect

International Journal of Impact Engineering

journal homepage: www.elsevier.com/locate/ijimpeng

Normal and oblique impact of small arms bullets on AA6082-T4 aluminium protective plates

Tore Børvik [a,b,*], Lars Olovsson [c], Sumita Dey [a,b], Magnus Langseth [a]

[a] Structural Impact Laboratory (SIMLab), Centre for Research-based Innovation (CRI) and Department of Structural Engineering, Norwegian University of Science and Technology, Rich. Birkelands vei 1A, NO-7491 Trondheim, Norway
[b] Norwegian Defence Estates Agency, Research and Development Section, PB 405 Sentrum, NO-0103 Oslo, Norway
[c] Impetus Afea AB, SE-14160 Huddinge, Sweden

ARTICLE INFO

Article history:
Received 19 June 2010
Received in revised form
26 January 2011
Accepted 1 February 2011
Available online 12 March 2011

Keywords:
Normal and oblique impact
Small arms bullets
Aluminium armour
3D numerical simulations

ABSTRACT

Normal and oblique impact on 20 mm thick AA6082-T4 aluminium plates are studied both experimentally and numerically. Two types of small arms bullets were used in the ballistic tests, namely the 7.62 × 63 mm NATO Ball (with a soft lead core) and the 7.62 × 63 mm APM2 (with a hard steel core), fired from a long smooth-bore Mauser rifle. The targets were struck at 0°, 15°, 30°, 45° and 60° obliquity, and the impact velocity was about 830 m/s in all tests. During testing, the initial and residual bullet velocities were measured by various laser-based optical devices, and high-speed video cameras were used to photograph the penetration process. Of special interest is the critical oblique angle at which the penetration process changes from perforation to embedment or ricochet. The results show that the critical oblique angle was less than 60° for both bullet types. A material test programme was also conducted for the AA6082-T4 plate to calibrate a modified Johnson–Cook constitutive relation and the Cockcroft–Latham failure criterion, while material data for the bullets mainly were taken from the literature. 3D non-linear FE simulations with detailed models of the bullets were finally run. Good agreement between the FE simulations and the experimental results for the APM2 bullets was in general obtained, while it was more difficult to get reliable FE results for the soft core Ball bullets.

1. Introduction

The need for protection against small arms and light weapons is large both from a civilian and a military point of view [1,2]. Even so, few investigations exist in the open literature where the hazard from such weapons has been systematically studied. The majority of ballistic studies are further concerned with the worst-case scenario, i.e. the normal impact condition where the angle between the velocity vector of the projectile and the normal vector of the target is zero. However, in most real cases the projectile will strike the target with some degree of obliquity. Earlier works on oblique impact have been collected in the review papers by Backman and Goldsmith [3], Johnson et al. [4], Corbett et al. [5] and Goldsmith [6]. Of these earlier works, the paper by Awerbuch and Bodner [7] is of particular interest. They showed experimentally that the velocity drop during perforation of aluminium plates by 0.22 calibre soft core lead bullets was almost unaffected by the oblique angle to around 30°. At higher oblique angles, the velocity dropped considerably. Similar results were obtained by Gupta and Madhu [8] for hard core steel bullets. More recent studies of oblique impacts on various materials can be found in Piekutowski et al. [9], Zhou and Stronge [10], Iqbal et al. [11,12], Teng et al. [13], Lopez-Puente et al. [14] and Shokrieh and Javadpour [15].

In this paper, normal and oblique impact on 20 mm thick AA6082-T4 aluminium plates are studied both experimentally and numerically. Two different types of small arms bullets were used in the ballistic tests, namely the 7.62 × 63 mm NATO Ball (with a soft lead core) and the 7.62 × 63 mm APM2 (with a hard steel core). The bullets were fired from a long smooth-bore Mauser rifle at a constant velocity of about 830 m/s in all tests. The targets were struck at 0°, 15°, 30°, 45° and 60° obliquity, and the critical oblique angle was determined. Initial and residual bullet velocities were accurately measured during testing by various laser-based optical devices, and two synchronized Photron Fastcam-Ultima APX high-speed video cameras were used to photograph the penetration process. A material test programme for the AA6082-T4 aluminium plate was conducted to identify the material parameters for the modified Johnson–Cook constitutive relation and the

* Corresponding author. Structural Impact Laboratory (SIMLab), Centre for Research-based Innovation (CRI) and Department of Structural Engineering, Norwegian University of Science and Technology, Rich. Birkelands vei 1A, NO-7491 Trondheim, Norway. Tel.: +47 73 59 46 47; fax: +47 73 59 47 01.
E-mail address: tore.borvik@ntnu.no (T. Børvik).

0734-743X/$ – see front matter © 2011 Elsevier Ltd. All rights reserved.
doi:10.1016/j.ijimpeng.2011.02.001

Cockcroft–Latham failure criterion. Material data for the bullets were mainly taken from the literature. 3D non-linear FE simulations with detailed models of the bullets were finally run and the different findings were compared against each other. While it was difficult to quantify FE results for the soft core Ball bullets, good agreement between the FE simulations and the experimental results for the hard core APM2 bullets was in general obtained.

2. Experimental tests

2.1. Target material

Extruded plates from Hydro Aluminium of the aluminium alloy 6082 in temper T4 were investigated. These plates were intended as lightweight replacements for concrete slabs as ballistic protective covers for buried cable trenches. Thus, impacts with oblique angles $60^\circ \le \beta < 90^\circ$ are most likely. The plate thickness was 20 mm in all tests. The AA6082 belongs to the AlMgSi series of alloys, where the major alloying elements are silicon (1.04 wt.%) and magnesium (0.67 wt.%), while the minor alloying elements are iron (0.2 wt.%) and manganese (0.54 wt.%). Temper T4 implies that the alloy is solution heat treated and naturally aged to a substantially stable condition [16].

Quasi-static tensile tests were carried out using smooth axisymmetric specimens [17] with a gauge length of about 40 mm and a cross-section diameter of 6 mm. The tensile axis of the specimens was oriented 0°, 45° and 90° with respect to the extrusion direction of the plate. Three parallel tests were carried out in each direction at room temperature and the scatter between parallel tests was found to be low. The cross-head velocity of the tension machine during testing was 1.2 mm/min, which corresponds to an average strain rate in the gauge area of $5 \times 10^{-4}\ s^{-1}$. The force and the diameter at minimum cross-section of the specimen were continuously measured until fracture. The latter was made possible using a purpose-built measuring rig with two perpendicular lasers that accurately measured the specimen diameter. The lasers were installed on a mobile frame to ensure that the diameter during straining always was measured at minimum cross-section. The specimen diameter was measured in the thickness direction (D_Z) of the plate and in the transverse direction ($D_\perp$) of the specimen. The Cauchy stress and the logarithmic strain were calculated as

$$\sigma = \frac{F}{A}, \quad \epsilon = \ln\frac{A_0}{A} \tag{1}$$

where F is the force, $A_0 = \pi/4D_0^2$ is the initial cross-section area and D_0 is the initial diameter of the gauge section. Due to possible variations in stress and strain over the cross-section, σ and ϵ should be considered as average values. The current area of the cross-section is

$$A = \frac{\pi}{4} D_Z D_\perp \tag{2}$$

The logarithmic plastic strain is then obtained as $\epsilon^p = \epsilon - \sigma/E$, where E is Young's modulus. Note that plastic incompressibility and negligible elastic strain have been assumed in Eq. (1), and that the measured Cauchy stress σ is equal to the major principle stress σ_1 in the uniaxial tension test. To account for the increased stress triaxiality in the material after diffuse necking, the Cauchy stress was corrected for triaxiality effects using Bridgman's analysis (see e.g. [1]) to obtain the equivalent stress σ_{eq}.

Typical Cauchy stress–logarithmic plastic strain curves until fracture are shown in Fig. 1 together with corresponding equivalent (Bridgman-corrected) stress–logarithmic plastic strain curves. It is noted that both the strength level and the logarithmic plastic strain to fracture differ markedly between the different directions. The highest fracture strain is found at 45° ($\epsilon_f = 0.88$), while the lowest fracture strain is found at 0° ($\epsilon_f = 0.53$). Thus, the material is clearly anisotropic both in strength and strain to fracture.

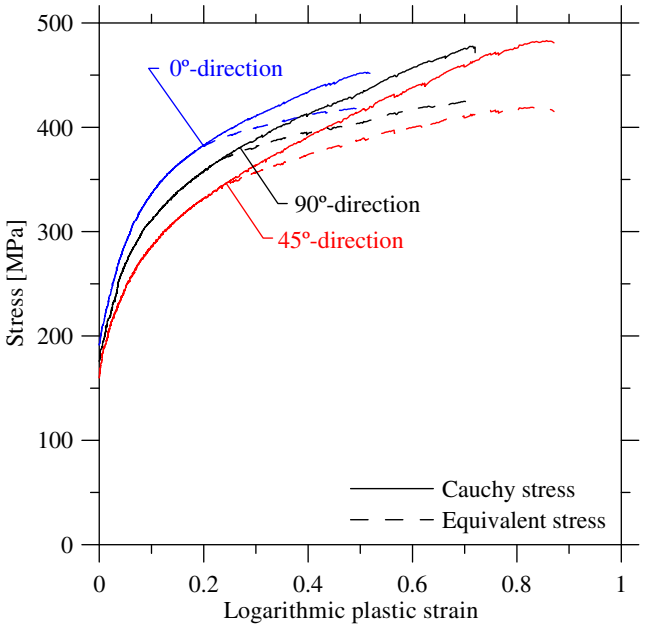

Fig. 1. Typical stress–strain curves from tension tests at room temperature and strain rate $5 \times 10^{-4}\ s^{-1}$ in three different directions to the extrusion direction of AA6082-T4. Both Cauchy stress and equivalent stress (Bridgman-corrected) versus logarithmic plastic strain are shown.

The strain-rate sensitivity of the alloy has not been checked experimentally in this study. However, Oosterkamp et al. [18] did uniaxial compression tests on AA6082 at strain rates from $0.1\ s^{-1}$ to $3000\ s^{-1}$. They found a very low, yet positive, increase in flow stress with strain rate at room temperature. Similar results for other aluminium alloys have been reported in the literature. Material data for the target material intended for numerical simulations will be presented in Section 4.

2.2. Bullet types

Both 7.62 mm NATO Ball bullets (with a soft lead core) and 7.62 mm 30-06 APM2 bullets (with a hard steel core) were used in the ballistic impact tests. Schematic drawings and geometries of the bullets are given in Fig. 2, where also the oblique angle β is defined. For the Ball bullet, the soft lead core is cast into a CuZn10 brass jacket. The lead is alloyed with 10% antimony to increase the strength of the core. For the APM2 bullet, the ogival nose (with a calibre-radius-head of 3) hard core projectile made of 1007 tool steel is inserted in a brass sabot, before the brass jacket with lead filler is clamped onto it. The various alloys in the Ball and APM2 bullets have been found to be almost identical [1]. The total mass of the Ball bullet is 9.5–10 g with a core mass of ~4.5 g, while the total mass of the APM2 bullet is 10.5–10.7 g with a core mass of ~5.0 g. The muzzle velocity of both bullets using a long smooth-bore Mauser rifle is roughly 900 m/s, and accordingly the initial kinetic energy is similar for the two bullet types. Thus, the only distinction in performance during impact is caused by the difference in core hardness. The muzzle velocity of the bullets is of minor importance in this study since the ammunition will be adjusted to a desired impact velocity before each test. A more thorough description of the bullet materials can be found in Børvik et al. [1],

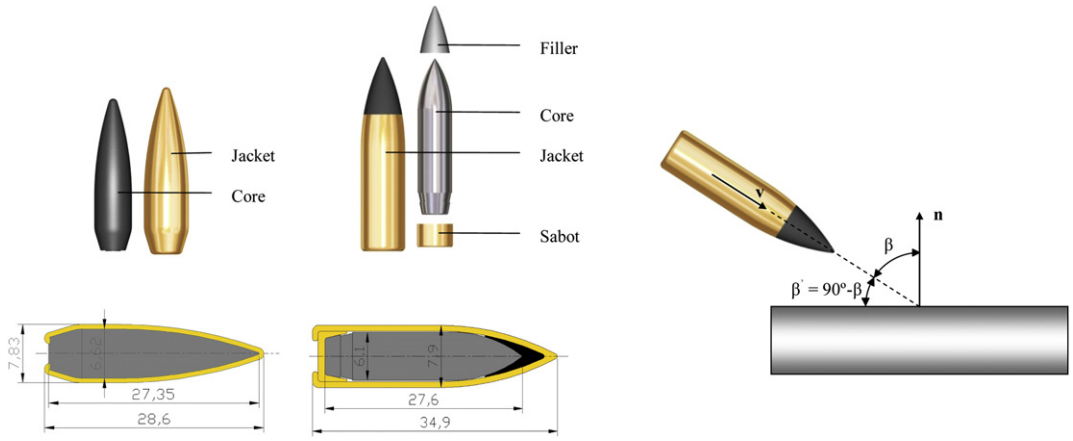

Fig. 2. Schematic drawings and geometries of bullets; 7.62 mm Ball and 7.62 mm APM2 (left) and definition of oblique angle and impact point (right).

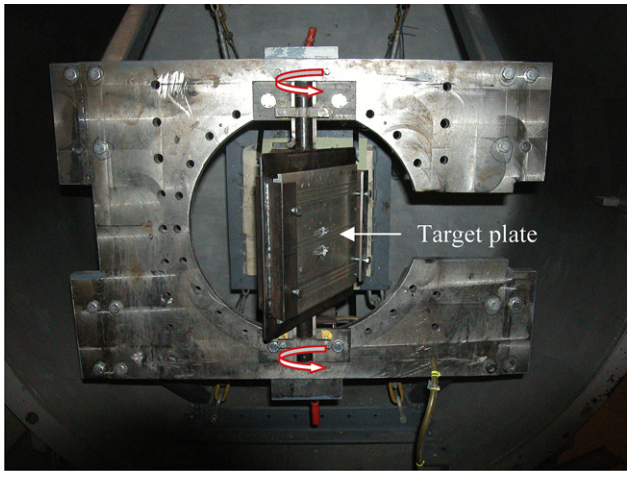

Fig. 3. Target plate mounted in the revolving frame.

while material data required for numerical simulations will be presented in Section 4.

2.3. Test set-up

The ballistic tests were carried out in a compressed gas gun facility described in more detail in Børvik et al. [19]. However, in these tests the gas gun itself was not used. Instead a 7.62 × 63 mm specially designed smooth-bored Mauser rifle with a barrel length of 1 m was used to fire the bullets [1]. During testing, the stock was removed and the rifle was mounted in a rigid rack inside a 16 m^3 impact chamber. This guaranteed a well-defined impact point in each test. The rifle was fired by a magnetic trigger from safe distance.

Target plates were mounted in a stiff frame and adjusted to the desired point of impact. Plates with dimension 300 × 300 mm^2 were firmly clamped to the revolving part of the frame by two beams and four bolts (see Fig. 3), before they were locked in the prescribed oblique position. This secured a fixed boundary of the vertical sides of the target, while the horizontal sides remained free. It is, however, assumed that the boundary conditions are of minor importance in high-velocity ballistic impacts if the in-plane distance between single shot and the boundary is more than several projectile diameters. Here, a maximum of 1–3 shots were allowed in each target before it was replaced. The test procedure

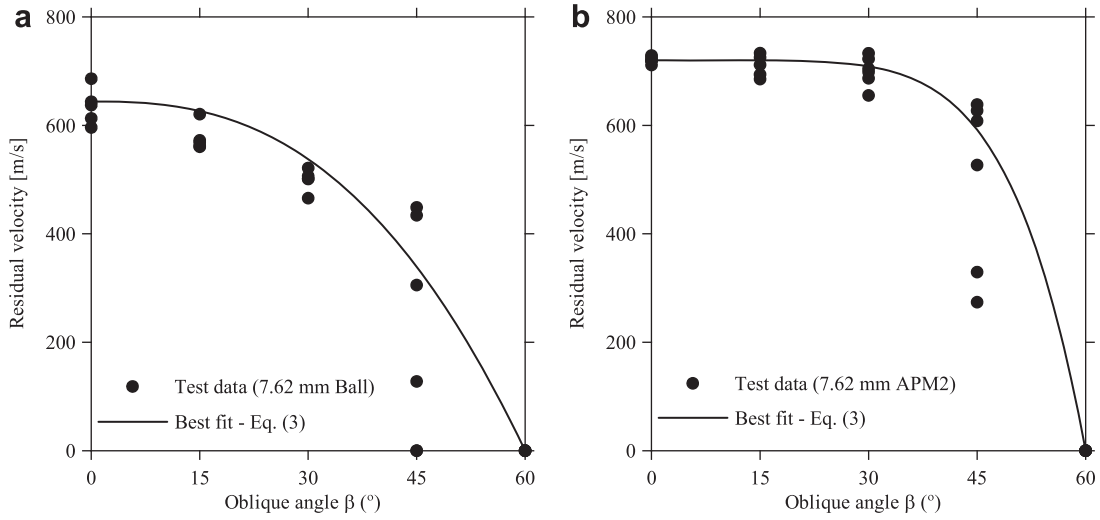

Fig. 4. Measured residual velocity versus oblique angle for a) Ball bullets and b) APM2 bullets.

followed in large the recommendations for ballistic testing given in various international norms and standards.

Two optical velocity measuring systems were available in the impact chamber to obtain the initial and residual projectile velocities [19]. To increase the accuracy and to get replicate measurements of the velocities, two extra chronographs were installed. The velocity measuring systems were validated by firing bullets through all 4 velocity stations without a target, and the spread in measured velocity was found to be within 1–2%. In addition, two synchronized Photron Fastcam-Ultima APX high-speed video cameras were used in some of the tests to photograph the penetration event at a constant framing rate of 90,000 fps.

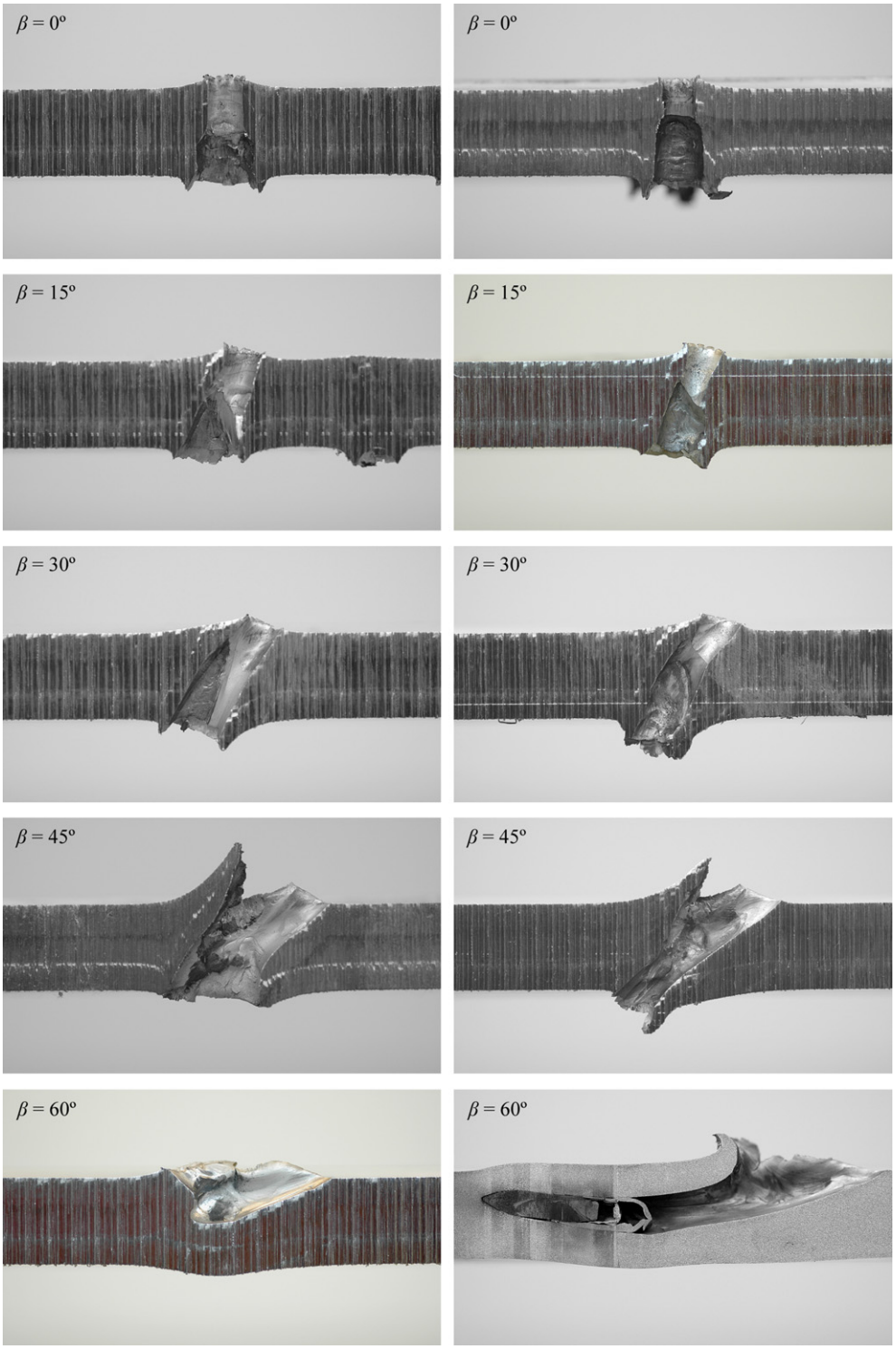

Fig. 5. Sliced target plates after impact of 7.62 mm Ball bullets (left) and 7.62 mm APM2 bullets (right) at increasing oblique angle β.

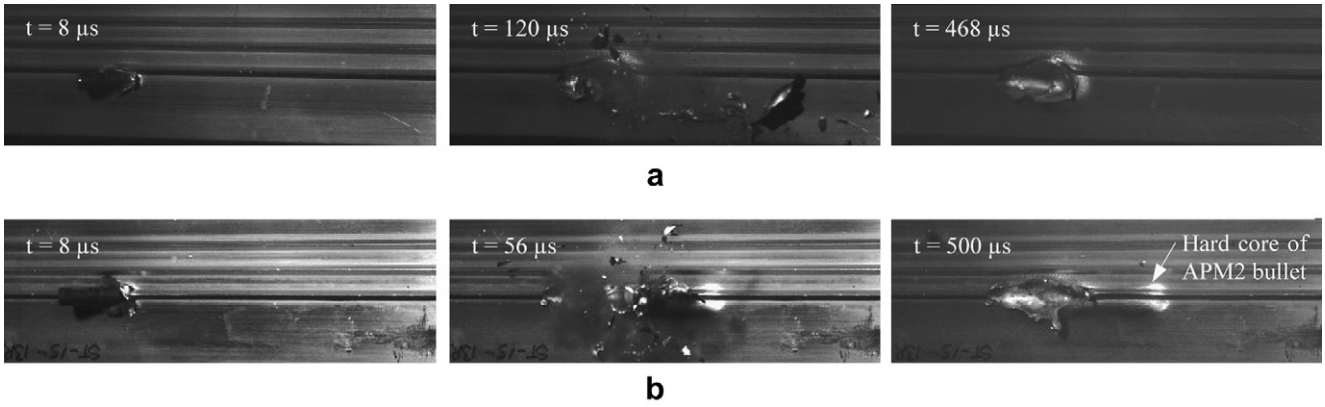

Fig. 6. Some high-speed camera images showing a) 7.62 mm Ball bullet and b) 7.62 mm APM2 bullet striking the front side of the aluminium plate at an oblique angle $\beta = 60°$.

3. Experimental results

Before each test the ammunition was adjusted to have a constant impact velocity of about 830 m/s to meet the requirements for protection class BR6 (7.62 mm soft core Ball bullets) and protection class BR7 (7.62 mm hard core AP bullets) in accordance with EN1063 [20]. This was done using earlier obtained adjustment graphs, relating the amount of powder in the cartridge to the measured muzzle speed of the bullet. Even though this was done with great care, significant spread (±20 m/s) in initial velocity was measured. This spread made it sometimes difficult to reach the predefined velocity of the bullet by a limited number of tests, and several repetitions were necessary.

Five to six tests were carried out for each bullet type and oblique angle. Fig. 4 gives measured residual velocity versus oblique angle from all tests assuming a constant initial velocity of 830 m/s. The experimental results for soft core Ball bullets show a continuous drop in residual velocity with oblique angle due to the increase of the effective plate thickness. For hard core AP bullets the experimental results were consistent with similar results from the literature, namely that the residual velocity is almost unaffected by oblique angle to about 30°. At higher oblique angles the velocity drop was extensive for both bullet types. The spread in results especially at an oblique angle of 45° will be further discussed in Section 5. Of special interest is the critical oblique angle, where the penetration process changes from perforation to ricochet or embedment. For this target the critical oblique angle is less than 60°. At higher oblique angles, none of the bullets were able to perforate the target plate.

The solid lines through the data points in Fig. 4 are based on best fits to the following simple interaction formula

$$\left(\frac{\beta}{C_1}\right)^m + \left(\frac{v_r}{C_2}\right)^n = 1 \;\rightarrow\; v_r = C_2\left[1 - \left(\frac{\beta}{C_1}\right)^m\right]^{1/n} \tag{3}$$

where v_r is the residual velocity of the actual bullet, β is the oblique angle and C_i are constants. By introducing the experimentally obtained boundary conditions for the soft core Ball bullet ($v_{r\ \mathrm{Ball}} \approx 640$ m/s when $\beta = 0°$ and $v_{r\ \mathrm{Ball}} = 0$ m/s when $\beta = 60°$) into Eq. (3), the constants C_1 and C_2 become 60° and 640 m/s, respectively. Similar, for the hard core APM2 bullet ($v_{r\ \mathrm{APM2}} \approx 720$ m/s when $\beta = 0°$ and $v_{r\ \mathrm{APM2}} = 0$ m/s when $\beta = 60°$), the constants C_1 and C_2 become 60° and 720 m/s, respectively. With these values, a best fit of Eq. (3) to the experimental data using the method of least squares gave $m = 2.6$ and $n = 1$ for the Ball bullet and $m = 6.0$ and $n = 1$ for the APM2 bullet. As seen from Fig. 4, reasonable agreements between the fits and the experimental data are obtained. Note that these fits should only be used to represent the data presented herein, and that the expression in Eq. (3) does not take the effects of projectile impact velocity or target material and thickness into account.

Pictures of some sliced target plates after impact at increasing oblique angle are shown in Fig. 5. Note that the cavities especially for $\beta = 0°$ change diameter after some penetration due to the deformation and stripping of the bullets' brass jacket. The cavities are somewhat wider for Ball bullets than for APM2 bullets (caused by the severe deformation of the Ball bullets upon impact). Except for this the cavities are similar and rather independent of bullet type. For $\beta = 60°$ the hard core of the APM2 bullet sometimes penetrated in the plane of the plate and was found embedded inside the target without rebound. The Ball bullet peeled off and ricocheted in all tests at this oblique angle.

Fig. 6 shows some high-speed camera images of Ball and APM2 bullets, respectively, during impact of the front side of the aluminium plate at an oblique angle $\beta = 60°$. The Ball bullet was completely destroyed during impact, and only some minor pieces of the jacket were found after the test. The hard core of the APM2 penetrated into the plate, but it did not pierce the rear side of the target (as shown in Fig. 5). Based on these test results it can be concluded that at oblique angles between 0° and 30° both bullet types perforate the target plate with a high residual velocity, at an oblique angle of 45° most bullets perforate (but some Ball bullets were stopped) the target plate with a large spread in residual velocity, while at an oblique angle of 60° all bullets are stopped.

Table 1
Material constants for the 0° direction for the target material.

Elastic constants and density			Yield stress and strain hardening				Strain rate hardening		Temperature softening and adiabatic heating						CL failure criterion
E (GPa)	ν	ρ (kg/m^3)	σ_0 (MPa)	A (MPa)	B (MPa)	n	$\dot{\epsilon}_0$ (s^{-1})	C	T_r (K)	T_m (K)	m	C_p (J/kg K)	χ	α (K^{-1})	W_{cr} (MPa)
70	0.3	2700	195.0	72.6	435.3	0.227	5×10^{-4}	0.001	293	893	1	910	0.9	2.3×10^{-5}	199

Table 2
Hardening constants and W_{cr} for the 45° and 90° directions for the target material.

Yield stress, strain hardening and W_{cr} (45° direction)					Yield stress, strain hardening and W_{cr} (90° direction)				
σ_0 (MPa)	A (MPa)	B (MPa)	n	W_{cr} (MPa)	σ_0 (MPa)	A (MPa)	B (MPa)	n	W_{cr} (MPa)
169.0	72.7	377.4	0.249	337	180.0	66.4	410.1	0.230	280

Table 3
Bullet material constants for the MJC constitutive relation and CL failure criterion.

Material	Yield stress	Strain hardening		Strain rate hardening		Temperature softening			CL
	A (MPa)	B (MPa)	n	$\dot{\epsilon}_0^*$ (s^{-1})	C	T_r (K)	T_m (K)	m	W_{cr} (MPa)
Hardened steel core	1200	50,000	1.0	5×10^{-4}	0	293	1800	1.0	–
Lead core and cap	24	300	1.0	5×10^{-4}	0.1	293	760	1.0	175
Brass jacket	206	505	0.42	5×10^{-4}	0.01	293	1189	1.68	914

4. Numerical simulations

4.1. Constitutive relation and failure criterion

A modified version of the Johnson–Cook (MJC) constitutive relation was used to model both the target and the bullet materials [17]. The constitutive behaviour of the materials is assumed to be isotropic and modelled with the von Mises yield criterion even though the target material exhibits strong anisotropy. The equivalent stress is expressed as

$$\sigma_{eq} = \left(A + B\epsilon_{eq}^{n}\right)\left(1 + \dot{\epsilon}_{eq}^{*}\right)^{C}\left(1 - T^{*m}\right) \tag{4}$$

where ϵ_{eq} is the equivalent plastic strain and A, B, n, C and m are material constants. The dimensionless plastic strain rate is given by $\dot{\epsilon}_{eq}^{*} = \dot{\epsilon}_{eq}/\dot{\epsilon}_0$, where $\dot{\epsilon}_0$ is a user-defined reference strain rate. The homologous temperature is defined as $T^{*} = (T - T_r)/(T_m - T_r)$, where T is the absolute temperature, T_r is the ambient temperature and T_m is the melting temperature. The temperature change due to adiabatic heating is calculated as

$$\Delta T = \int_0^{\epsilon_{eq}} \chi \frac{\sigma_{eq}\, d\epsilon_{eq}}{\rho C_p} \tag{5}$$

where ρ is the material density, C_p is the specific heat and χ is the Taylor–Quinney coefficient that represents the proportion of plastic work converted into heat.

Failure is modelled using a criterion proposed by Cockcroft and Latham (CL) [21]

$$W = \int_0^{\epsilon_{eq}} \langle\sigma_1\rangle\, d\epsilon_{eq} \le W_{cr} \tag{6}$$

where σ_1 is the major principal stress, $\langle\sigma_1\rangle = \sigma_1$ when $\sigma_1 \ge 0$ and $\langle\sigma_1\rangle = 0$ when $\sigma_1 < 0$. From Eq. (6) it is seen that failure cannot occur when there is no tensile stress operating. The critical value of W, denoted W_{cr}, can be determined from a simple uniaxial tensile test. It was shown by Dey et al. [22,23] that the one-parameter CL criterion gives equally good results as the five-parameter MJC failure criterion in LS-DYNA simulations of perforation of steel plates under various stress states using different projectile nose shapes. It should however be noted that owing to the anisotropy of the material and the uncertainty in the calibration of the CL criterion, W_{cr} should not be regarded as a material characteristic. The criterion is here only intended for design. In this study, the deviatoric stresses in the element are set to zero when W reaches its critical value W_{cr} at a specific integration point. This is defined as material failure. However, the element continues to take compressive stresses until the time step size drops below a critical level. This is defined as material erosion. The constitutive relation and the failure criterion have been implemented in the non-linear explicit finite element code IMPETUS Afea Solver [24].

Table 4
General material constants for the MJC constitutive relation.

Material	E (MPa)	ν	ρ (kg/m^3)	C_p (J/kg K)	χ	α (K^{-1})	T_c^*
All steel alloys	210,000	0.33	7850	452	0.9	1.2×10^{-5}	0.9
Lead core and cap	1000	0.42	10,660	124	0.9	2.9×10^{-5}	0.9
Brass jacket	115,000	0.31	8520	385	0.9	1.9×10^{-5}	0.9

4.2. Identification of material constants

The hardening parameters A, B and n in the various material directions of the target were first determined by best fits to the test data in Fig. 1 using the method of least squares. For this material, the Johnson–Cook hardening term provides a rather poor fit. Owing to the lack of tensile test data at elevated strain rates and temperatures, the material parameter C was given a small positive value [18], while $\dot{\epsilon}_0$ was taken equal to the strain rate in the quasi-static tensile tests. Further, the material parameter m was set to unity, implying a linear decrease in flow stress with increasing temperature.

The fracture parameter W_{cr} was identified by using that in uniaxial tension $W_{cr} = \int_0^{\epsilon_f} \sigma\, d\epsilon^p$. Material parameters for AA6082-T4 obtained from tensile tests in the 0° direction are given in Table 1. These data will be applied in the bulk of the numerical

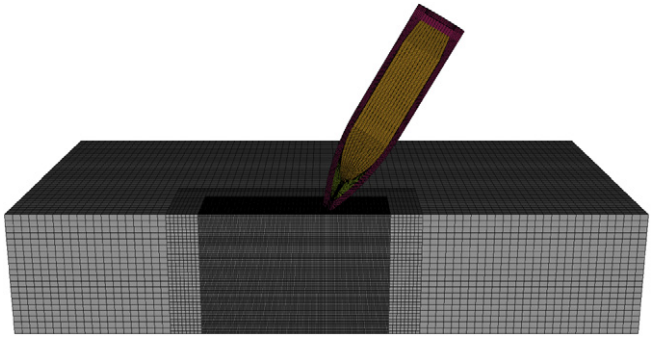

Fig. 7. Plot of a typical initial mesh for the fine model (7.62 mm APM2 bullet; 20 mm thick aluminium plate; oblique angle $\beta = 30°$). The model has been cut in half to show the interior.

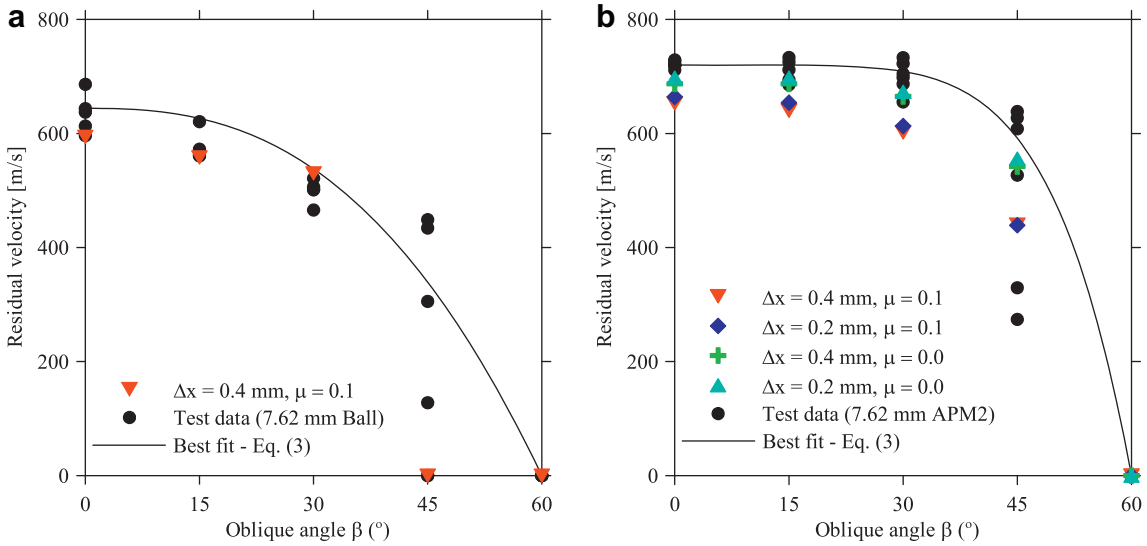

Fig. 8. Residual velocity versus oblique angle for a) Ball and b) APM2 bullets: Comparison between experimental data and numerical results (using material constants in the 0° direction for AA6082-T4).

simulations. However, to check the possible effect of anisotropy on the predictions, hardening and fracture parameters determined from tensile tests in the 45° and 90° directions are given in Table 2. Material constants for the various bullet materials were taken from Børvik et al. [1], and are listed in Tables 3 and 4. Physical constants for the various materials were given nominal values provided in the literature.

4.3. Numerical models

All numerical simulations were carried out using the explicit finite element code IMPETUS Afea Solver [24]. The projectile and the region in the target plate that undergoes large deformations were modelled using fully integrated 3rd-order 64-node hexahedrons. Since the size of the impact region increased with oblique angle, a larger zone with higher-order elements was required at large oblique angles. Eight-noded selectively reduced integrated hexahedrons were used in less crucial parts of the target plate. Geometries of the target and bullets were similar to those used in the tests (see [1] for details regarding the various bullets nominal mass and geometry), except that the target was modelled somewhat smaller than in the test to save computational time. The target was also modelled as fully clamped along the boundaries. The impact velocity was taken as 826.8 m/s for Ball bullets and 833.6 m/s for APM2 bullets. These values are average velocities based on a large number of experimental tests. In addition, two different target plate mesh densities were used in the numerical simulations; one coarse model with node spacing $\Delta x = \Delta y = \Delta z = 0.4$ mm and one fine model with node spacing $\Delta x = \Delta y = \Delta z = 0.2$ mm in the impact region. Using these sizes, the number of nodes varied between 600,000 and 800,000 for the coarse models, while for the fine models the number of nodes was between 1.5 and 2.6 millions. A plot of the initial mesh for a fine model is shown in Fig. 7.

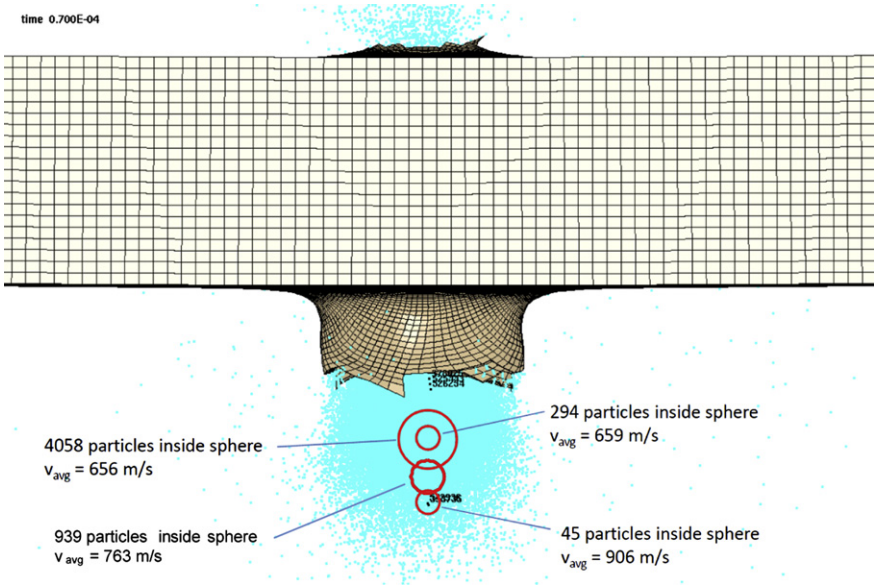

Fig. 9. Residual velocity measurement for Ball bullets.

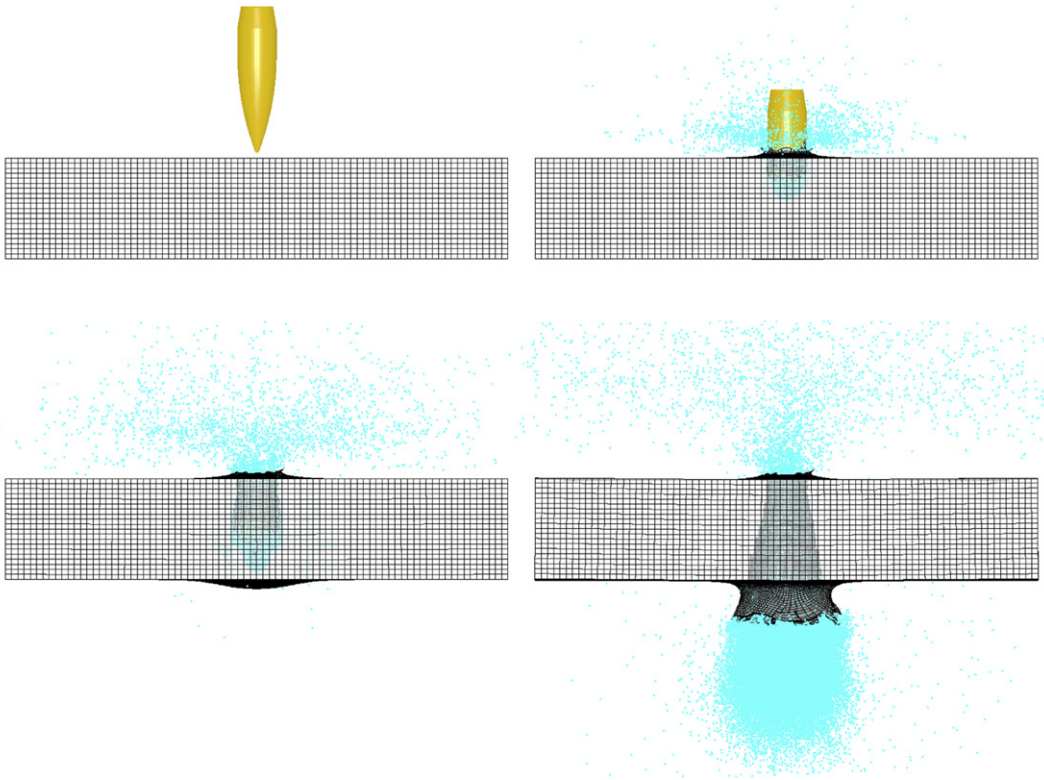

Fig. 10. Some plots from numerical simulations showing a 7.62 mm Ball bullet during impact of the aluminium plate at an oblique angle $\beta = 0^\circ$.

The constitutive behaviour was modelled using the MJC relation given by Eq. (4), while material failure was modelled using the CL failure criterion defined in Eq. (6). All required material parameters for the target and bullets are given in Tables 1–4. Most simulations were run with material constants for the target based on tensile tests in the 0° direction (Table 1), while some simulations were run with hardening and failure parameters for the target based on tensile tests in the 45° direction (Table 2). This was done to get a check of the possible effect of material anisotropy on the predictions. Note that the constants for the 45° direction give lower strength and higher ductility of the material than the constants for the 0° direction (see Fig. 1). As the material failed, all deviatoric

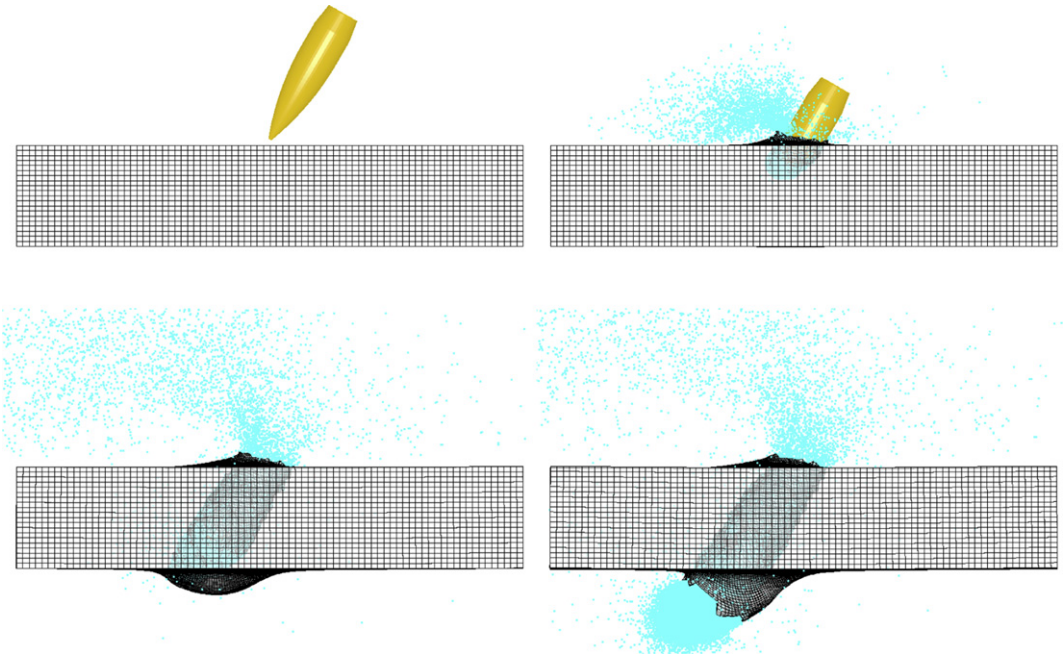

Fig. 11. Some plots from numerical simulations showing a 7.62 mm Ball bullet during impact of the aluminium plate at an oblique angle $\beta = 30^\circ$.

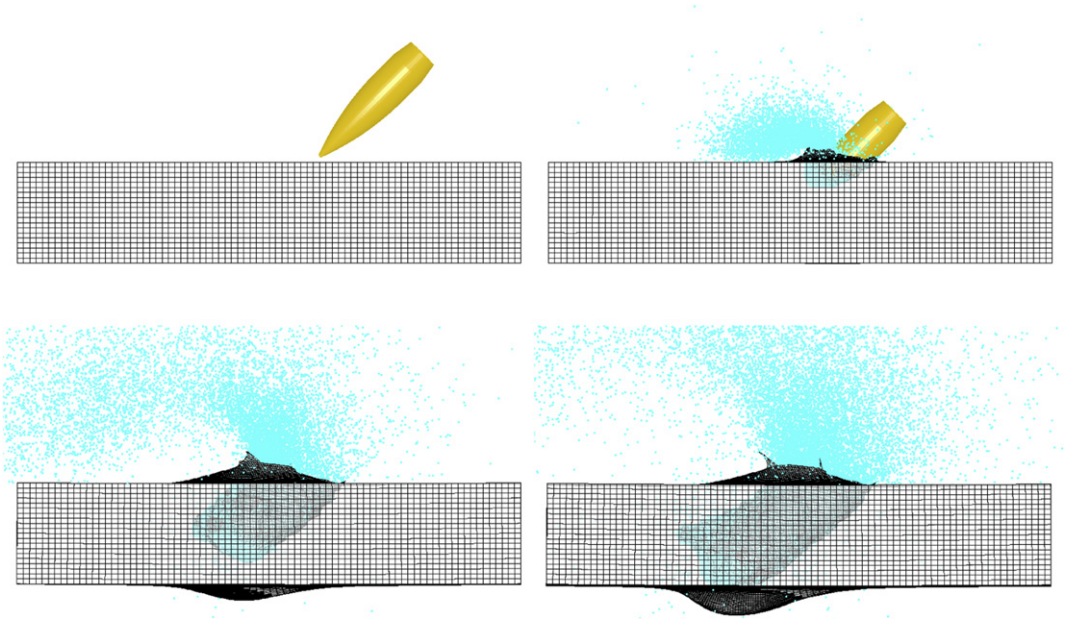

Fig. 12. Some plots from numerical simulations showing a 7.62 mm Ball bullet during impact of the aluminium plate at an oblique angle $\beta = 45°$.

stresses were set to zero. However, the material was still allowed to take compressive stresses and failed elements were not eroded until their time step dropped below a user-defined critical level. Element erosion was used to prevent overly distorted elements which reduce the time step towards zero and could cause error termination. In the coarse target model, the critical time step for element erosion was taken equal to 10 ns, whereas in the fine target model and in the bullets the critical time step for element erosion was taken equal to 5 ns. This approach sometimes eroded a few overly deformed elements in the pointed nose of the hard core AP bullet, but this is not expected to have any significant influence on the final results. The material's ability to take compressive stresses after failure was found to be of particular importance in the simulations of the soft core Ball bullets that were completely shattered during impact.

Contact between the various parts was established using a penalty-based node-to-surface algorithm. In the current work, all exterior nodes and element faces were active in the contact. Free nodes of failed elements kept their mass and momentum, and remained active in the contact. Being given a physical radius to correctly represent the volume of eroded elements, free nodes were also in contact with each other. A somewhat similar approach was proposed by Johnson and Stryk [25]. The effect of friction was studied by changing the frictional coefficient in the contact

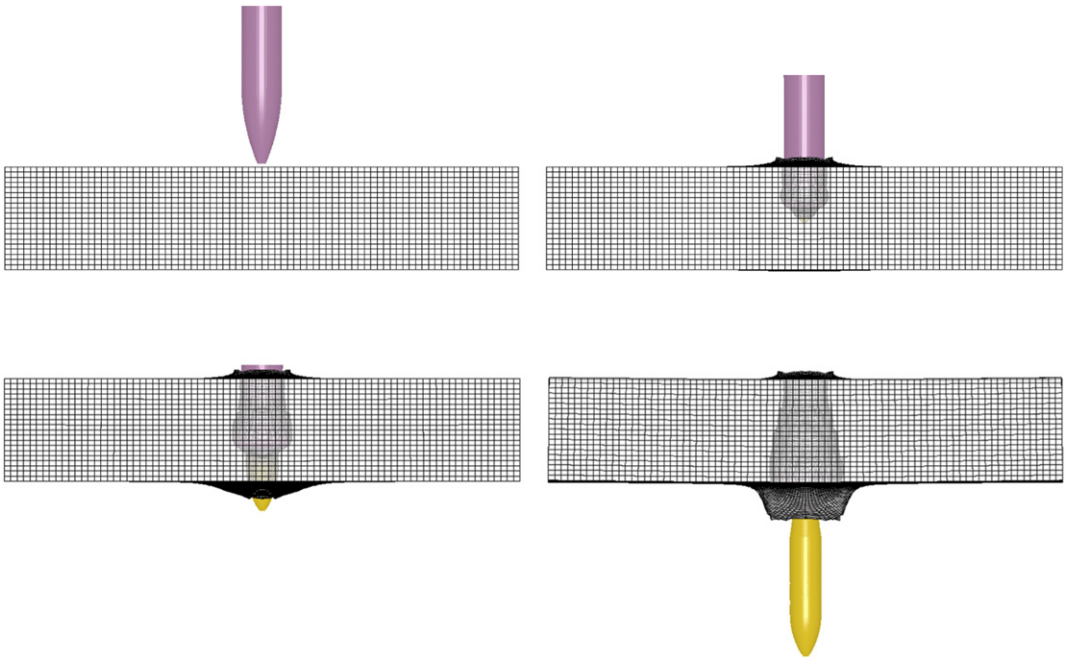

Fig. 13. Some plots from numerical simulations showing a 7.62 mm APM2 bullet during impact of the aluminium plate at an oblique angle $\beta = 0°$.

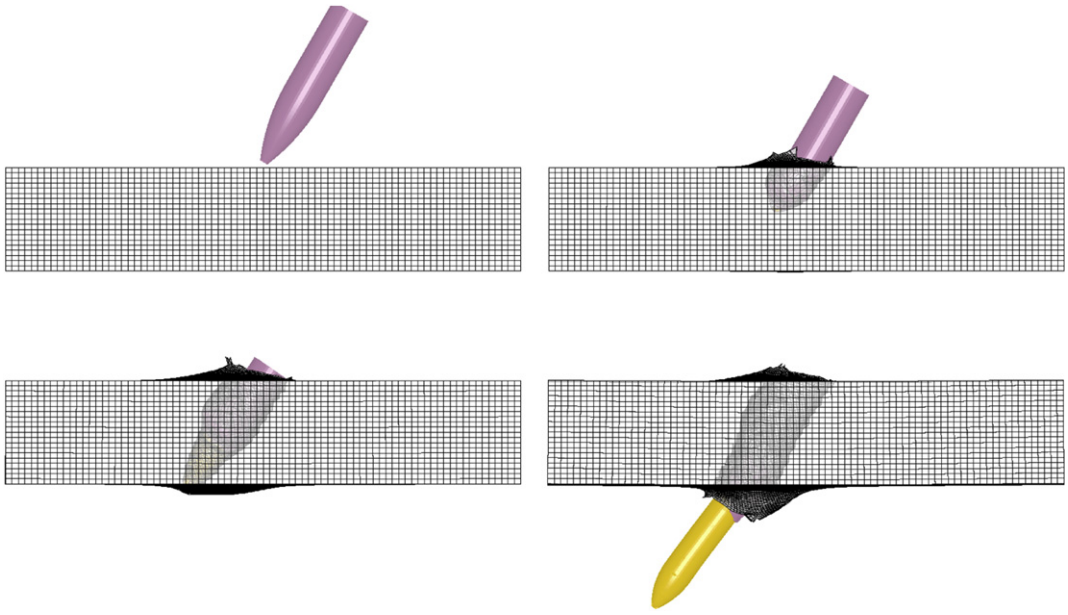

Fig. 14. Some plots from numerical simulations showing a 7.62 mm APM2 bullet during impact of the aluminium plate at an oblique angle $\beta = 30°$.

algorithm, and two different values ($\mu = 0$ and $\mu = 0.1$) were applied in the simulations.

4.4. Numerical results

Numerical results using the models described above are plotted and compared with the experimental data in Fig. 8. Results from the Ball bullets are considered first. In a similar way as in [1], it was found difficult to get reliable velocity measurements of the soft core bullets after perforation. Due to the low strength of the lead core, it failed almost immediately after impact (as in the experiments). Since the nodes of all these failed elements kept their mass and momentum, and were still active in the contact, they generated a cloud of impacting particles that eventually perforated the target. However, it was hard to extract the overall residual velocity from this cloud of particles due to the large spread in single node velocity (see Fig. 9). Only one of the 4 simulated cases is therefore plotted in Fig. 8(a), and these results must be considered as average values. The simulated critical oblique angle was found to be 45°, in contrast to the experimentally obtained critical angle of 60° (even though some of the soft core bullets were stopped at $\beta = 45°$ also experimentally). Thus, the numerical results for Ball bullets are non-conservative. Plots from some simulations ($\Delta x = 0.4$ mm, $\mu = 0.1$) involving Ball bullets at various oblique angles are shown in Figs. 10–12. Even though it was hard to measure the residual velocity of the particle cloud exactly, the overall behaviour is well predicted if compared to Fig. 5.

Results from the APM2 bullets are presented in Fig. 8(b). It was easy to measure the residual velocity of the hard steel core, and results from all 4 cases are therefore plotted. The numerical results are in close agreement with the experimental data. The simulated critical oblique angle was found to be 60°, as in the experiments. The data further indicate that while the effect of mesh density is small, the effect of friction is more distinct. The best results were obtained if no friction was assumed, i.e. $\mu = 0$. Under such conditions, the numerical data are within the experimental spread. Plots from some

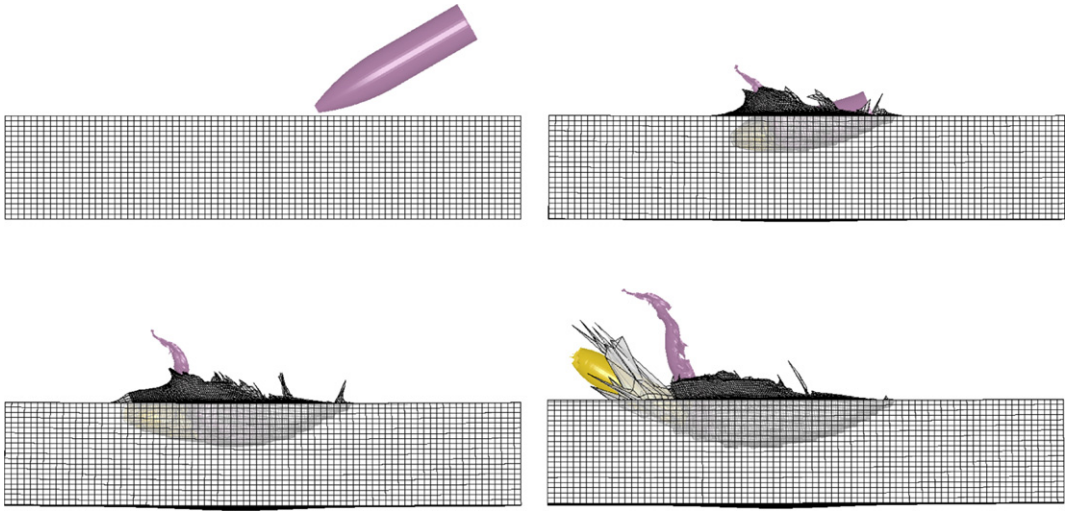

Fig. 15. Some plots from numerical simulations showing a 7.62 mm APM2 bullet during impact of the aluminium plate at an oblique angle $\beta = 60°$. Both overly deformed elements and some erosion in the hard core nose of the APM2 bullet are seen in this simulation.

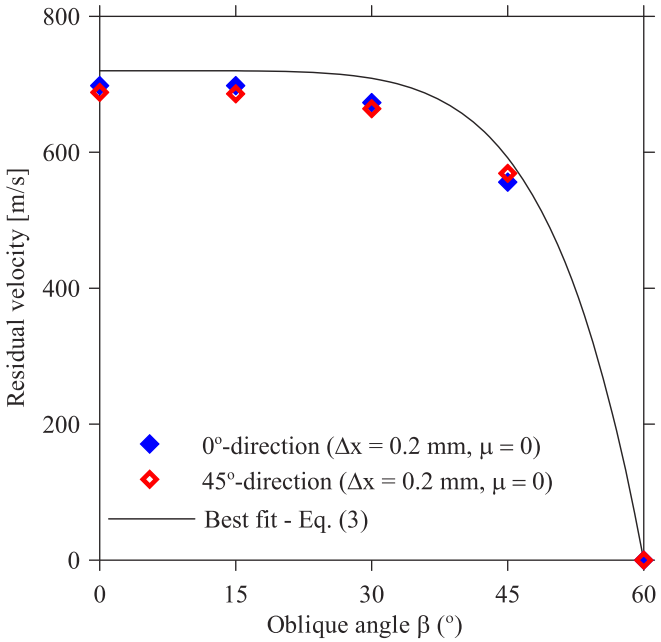

Fig. 16. Effect of material direction (0° and 45°) on the predicted residual velocity versus oblique angle for APM2 bullets.

simulations ($\Delta x = 0.4$ mm, $\mu = 0.1$) using APM2 bullets at various oblique angles are shown in Figs. 13–15. Again, the overall behaviour during impact is well predicted if compared to Fig. 5. Nodes of failed elements are not shown in these figures due to clarity, but the number was far less than in corresponding simulations using Ball bullets. Note also the overly distorted elements in Fig. 15. These elements have failed, but were not eroded.

Finally, to get a check of the possible effect of material anisotropy on the numerical predictions, some simulations with $\Delta x = 0.2$ mm and $\mu = 0$ were run with material constants from the 45° direction (Table 2) and compared with those obtained using data from the 0° direction (Table 1). The results are plotted in Fig. 16. Hardly any effect of material direction on the perforation resistance is observed. This is consistent with earlier observations during normal impact of AA7075-T651 aluminium plates [26]. The main reason for this result seems to be the strong strain localisation in this particular problem. Since the damage grows exponentially in the localised elements, the critical value of W becomes less important and material failure is reached within a few time steps. However, the effect of material anisotropy during ballistic impact is complex and requires further studies.

5. Discussion

From the experimental results presented in Section 3 it was found that the residual velocity of the hard core AP bullet is almost constant up to about 30° obliquity even though the penetration path increases by approximately 15%. Similar results have been obtained in other studies (see e.g. [8,11,12]). At low oblique angles the perforation resistance of the target to the applied load is very limited (i.e. the velocity drop of the bullet during perforation is less than 15%). The reason for this is that a small change in target thickness will not significantly affect the residual velocity of the bullet when the impact velocity is well above the ballistic limit [27]. However, as the oblique angle is approaching the critical angle, substantial spread in the experimental results is seen. A critical point is reached where a small change in impact angle, impact velocity or pitch/yaw of the bullet leads to a different path, making the process change from perforation with a relatively high residual velocity to ricochet. In this specific case, the critical point is close to an impact angle of 45°. At an oblique angle of 60°, the bullet just slides over the target surface causing cavitation before it rebounds without perforation. Also the numerical simulations are sensitive to small changes in impact conditions. Fig. 17 shows some plots where the perforation problem in Fig. 15 is simulated with a decrease in oblique angle of 2° and an increase in impact velocity of 2%. Under such conditions the hard core of the APM2 bullet penetrates in the plane of the plate in an exactly similar manner as seen experimentally (see Fig. 5). If the oblique angle is further decreased, the bullet will eventually perforate the target.

It was shown in Section 4 that the proposed numerical models were able to predict the normal and oblique impact of small arms bullets on aluminium protective plates. These results were obtained using a rather simple isotropic constitutive relation and failure criterion for the clearly anisotropic target material. It was also found that the perforation resistance was barely affected by material direction used in the identification of material constants. Similar results have been obtained in other impact studies involving simplified material models for complex problems (see e.g. [1,23,26]). A possible explanation for this is that the higher flow stress in the 0° direction counterbalance the lower fracture strain compared to the 45° direction in this particular problem (involving high initial pressures and extreme localisation in the impacted region). This behaviour is for the time being not clear and requires further studies.

As discussed in Section 4.3, nodes of eroded elements are not deactivated in the simulations. To check the effect of using this approach, simulations were run both with and without this algorithm activated. For the APM2 bullets, where the number of failed

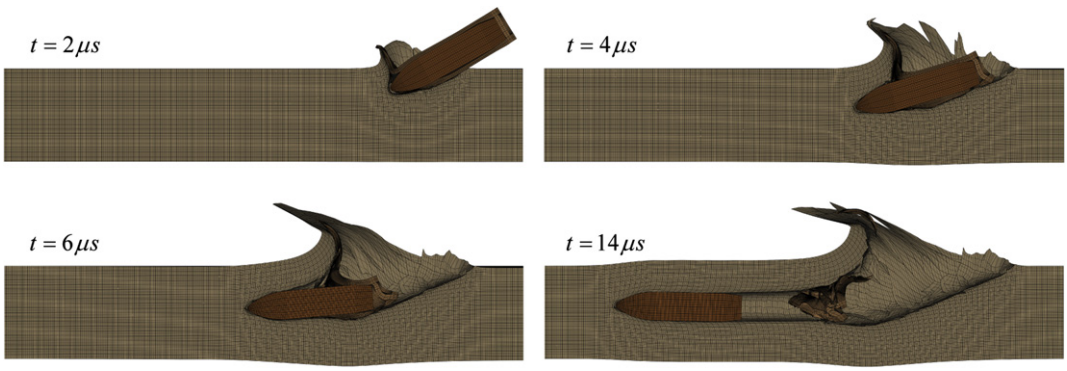

Fig. 17. Some plots from numerical simulations showing a 7.62 mm APM2 bullet during impact of the aluminium plate at an oblique angle $\beta = 58°$. The model has been cut in half to show the interior.

elements is low, the numerical results were hardly affected by the free nodes. For Ball bullets, however, where the soft core failed almost immediately after impact, it was vital that the free nodes kept their mass, momentum and contact. If not, the bullet material just eroded during impact rather than moving the target material out laterally in a ductile hole-growth mode. Under such conditions, the energy loss during perforation becomes unacceptable. When the nodes of eroded elements are active, this is no longer a problem, and the simulations are more realistic.

It is also of interest to compare the experimental results for this alloy against similar results for other aluminium alloys when $\beta = 0$, i.e. under normal impact conditions. Table 5 gives a collection of test results for 20 mm thick AA6082-T4, AA5083-H116 and AA7075-T651 plates when struck by 7.62 mm Ball or APM2 bullets at comparable impact velocities. The data for APM2 bullets are taken from Børvik et al. [28] and Forrestal et al. [29], while the data for Ball bullets are previously unpublished results. The yield stress σ_0 in the 0° direction for the various alloys is approximately 195 MPa for AA6082-T4, 230 MPa for AA5083-H116 and 520 MPa for AA7075-T651. The results indicate that the ballistic limit velocity increases monotonically with yield stress, but not as much as the difference in yield stress should imply. For the soft core Ball bullet, an increase in ballistic limit of more than 50% is expected when AA6082-T4 is replaced with the harder AA7075-T651 having the same weight and thickness. The reason for this is that the harder the plate, the more deformation is forced onto the soft core bullet at impact. The consequence is that the Ball bullet gradually looses its perforation ability with target hardness. For the hard core AP bullet, where the core is significantly harder than the target material, the corresponding increase in ballistic limit is less and around 30%. Here, the perforation resistance is mainly controlled by the target's resistance to plastic flow in the radial direction, and hardly any energy is dissipated in bullet deformation.

Computer codes divide the deformation of metals into volumetric (hydrostatic) and shear (deviatoric) parts. In dynamic problems, the material's shear strength is typically described by a pressure-independent thermoviscoplastic constitutive relation, while the hydrostatic pressure is described in terms of an equation-of-state (EOS) that relates pressure to relative volume and some thermal parameter. The significance of the EOS depends on the pressure (which again is a function of the impact velocity). For small pressures, it relates the pressure to the volumetric strain through the elastic bulk modulus (i.e. a linear relation between pressure and volumetric strain). For higher pressures the effect of the internal energy can be significant, and the relation between pressure and volumetric strain may be non-linear [30,31]. It is therefore necessary to solve the pressure and internal energy equations simultaneously to ensure that the pressure and energy are consistent. When the impact velocity of the striker is increased from low to high, it becomes important to evaluate the need for a non-linear EOS. For inert solids impact, the Mie-Grüneisen non-linear EOS is commonly used. This EOS may be written as (see also [30–32]).

Table 5
Comparison of ballistic impact test results for different aluminium alloys.

Aluminium alloy	Hard core APM2 bullets			Soft core Ball bullets		
	v_i [m/s]	v_r [m/s]	v_{bl} [m/s]	v_i [m/s]	v_r [m/s]	v_{bl} [m/s]
AA6082-T4	830.5	720.0	413.9*	829.5	596.2	576.7[a]
AA5083-H116	822.4	694.3	492.2	814.1	485.3	666.8
AA7075-T651	824.6	561.8	627.6	813.2	209.1	741.0

[a] Estimated values based on the Recht–Ipson model assuming $p = 1$ and $a = 2$, i.e. $v_{bl} = \sqrt{v_i^2 - v_r^2}$.

$$p(\rho, e) = p_0(1 - \Gamma\eta) + \frac{\rho_0 c_0^2 \eta}{(1 - s\eta)} \cdot \left(1 - \frac{\Gamma\eta}{2}\right) + \Gamma\rho_0(e - e_0) \tag{7}$$

with

$$\eta = 1 - \frac{\rho_0}{\rho} \tag{8}$$

where p is the pressure, ρ is the density, Γ is the Grüneisen gamma, c_0 is the elastic wave speed, s is the linear Hugoniot slope coefficient and e is the internal energy. This form of the non-linear Mie-Grüneisen EOS was implemented in the IMPETUS Afea Solver, and used in simulations of the APM2 bullet ($v_i = 833.6$ m/s, $\beta = 0$, $\mu = 0.1$ and $\Delta x = 0.4$ mm). The following material constants were used as input to the model [32,33]; $p_0 = e_0 = 0$, $c_0 = 5092$ m/s, $\Gamma = \Gamma_0 = 1.97$ and $s = 1.4$. The residual velocity of the hard core bullet was found to be 649 m/s using the non-linear EOS, while the corresponding residual velocity using the linear EOS was 651 m/s. These results are in agreement with Zukas et al. [34] who stated that "*only moderate pressures (300–500 kb) are generated for solid–solid impacts in the 0.5–2 km/s velocity regime, and the pressure decays rapidly to values comparable to the strength of the material. Hence, the equation-of-state under such impact conditions is of secondary importance*". The effect of using a linear versus a non-linear EOS in the velocity regime 833.6 m/s $\leq v_i \leq$ 6668.8 m/s is discussed in more detail by Børvik et al. [35].

6. Concluding remarks

Normal and oblique impact of small arms bullets on 20 mm thick AA6082-T4 aluminium plates have been studied experimentally and numerically. Two different types of bullets were used in the ballistic tests, namely the 7.62 × 63 mm NATO Ball (with a soft lead core) and the 7.62 × 63 mm APM2 (with a hard steel core). The targets were struck at 0°, 15°, 30°, 45° and 60° obliquity, and the impact velocity was about 830 m/s in all tests. The experimental results for the hard core bullets showed that the velocity drop during perforation is almost unaffected by oblique angle to about 30°. For soft core bullets a more continuous drop in velocity with oblique angle was observed. At the highest oblique angles the velocity drop was considerable and the critical oblique angle was less than 60° for both bullet types. At higher oblique angles, none of the bullets were able to perforate the target plate.

A modified Johnson–Cook constitutive relation and the Cockcroft–Latham failure criterion were calibrated based on material tests and used in 3D non-linear FE simulations of the impact problem. Good agreement between the FE simulations and the experimental results was obtained for the APM2 bullets, while it was more difficult to get reliable FE results for the soft core Ball bullets. It was found pivotal that free nodes from failed elements kept their mass, momentum and contact in simulations of the Ball bullets to obtain reliable results. The possible effect of material anisotropy on the predictions was also checked, but material direction was found to be of minor importance at all oblique angles. Finally, the effect of using a linear versus a non-linear EOS in this velocity regime was investigated. No noticeable difference between simulations using a linear versus a non-linear EOS was found. Hence, the form of the EOS seems to be of secondary importance in this particular problem.

Acknowledgement

The financial support of this work from the Structural Impact Laboratory (SIMLab), Centre for Research-based Innovation (CRI) at the Norwegian University of Science and Technology, is gratefully acknowledged.

References

[1] Børvik T, Dey S, Clausen AH. Perforation resistance of five different high-strength steel plates subjected to small-arms projectiles. International Journal of Impact Engineering 2009;36:948–64.

[2] Cheeseman A, Gooch WA, Burkins MS. Ballistic evaluation of aluminum 2139-T8. In: Bless SJ, Walker JW, editors. Proceedings of the 24th international symposium on ballistics, September 2008, New Orleans, USA; 2008. p. 651.

[3] Backman EM, Goldsmith W. The mechanics of penetration of projectiles into targets. International Journal of Engineering Science 1978;16:1–99.

[4] Johnson W, Sengupta AK, Ghosh SK. High velocity oblique impact and ricochet mainly of long rod projectiles; an overview. International Journal of Impact Engineering 1982;24:425–36.

[5] Corbett GG, Reid SR, Johnson W. Impact loading of plates and shells by free-flying projectiles: a review. International Journal of Impact Engineering 1996;18:141–230.

[6] Goldsmith W. Non-ideal projectile impact on targets. International Journal of Impact Engineering 1999;22:95–395.

[7] Awerbuch J, Bodner SR. An investigation of oblique perforation of metallic plates by projectiles. Experimental Mechanics 1977;17:147–53.

[8] Gupta NK, Madhu V. Normal and oblique impact of a kinetic energy projectile on mild steel plates. International Journal of Impact Engineering 1992;12:333–44.

[9] Piekutowski AJ, Forrestal MJ, Poormon KL, Warren TL. Perforation of aluminum plates with ogive-nose steel rods at normal and oblique impacts. International Journal of Impact Engineering 1996;18:877–87.

[10] Zhou DW, Stronge WJ. Ballistic limit for oblique impact of thin sandwich panels and spaced plates. International Journal of Impact Engineering 2008;35:1339–54.

[11] Iqbal MA, Gupta G, Gupta NK. 3D numerical simulations of ductile targets subjected to oblique impact by sharp nose projectiles. International Journal of Solids and Structures 2010;47:224–37.

[12] Iqbal MA, Chakrabarti A, Beniwal S, Gupta NK. 3D numerical simulations of sharp nosed projectile impact on ductile targets. International Journal of Impact Engineering 2010;37:185–95.

[13] Teng TL, Chu YA, Chang FA, Chin HS. Numerical analysis of oblique impact on reinforced concrete. Cement and Concrete Composites 2005;27:481–92.

[14] Lopez-Puente J, Zaera R, Navarro C. Experimental and numerical analysis of normal and oblique ballistic impacts on thin carbon/epoxy woven laminates. Composites Part A 2008;39:374–87.

[15] Shokrieh MM, Javadpour GH. Penetration analysis of a projectile in ceramic composite armor. Composite Structures 2008;82:269–76.

[16] Hatch JE. Aluminium: properties and physical metallurgy. Metals Park, Ohio: American Society for Metals; 1984.

[17] Børvik T, Hopperstad OS, Berstad T, Langseth M. A computational model of viscoplasticity and ductile damage for impact and penetration. European Journal of Mechanics – A/Solids 2001;5:685–712.

[18] Oosterkamp LD, Ivankovic A, Venizelos G. High strain rate properties of selected aluminium alloys. Materials Science and Engineering A 2000;278:225–35.

[19] Børvik T, Hopperstad OS, Langseth M, Malo KA. Effect of target thickness in blunt projectile penetration of Weldox 460 E steel plates. International Journal of Impact Engineering 2003;28(4):413–64.

[20] European Standard. Glass in building, security glazing, testing and classification of resistance against bullet attack. EN 1063; November, 1999.

[21] Cockcroft MG, Latham DJ. Ductility and workability of metals. Journal of the Institute of Metals 1968;96:33–9.

[22] Dey S. High-strength steel plates subjected to projectile impact. Ph.D. thesis; 2004. p. 38 (ISBN 82-471-6282-2). Department of Structural Engineering, Norwegian University of Science and Technology, Norway.

[23] Dey S, Børvik T, Hopperstad OS, Langseth M. On the influence of fracture criterion in projectile impact of steel plates. Computational Materials Science 2006;38:176–91.

[24] http://www.impetus.no/ [cited 100610].

[25] Johnson G, Stryk RA. Conversion of 3D distorted elements into meshless particles during dynamic deformation. International Journal of Impact Engineering; 2003:947–66.

[26] Børvik T, Hopperstad OS, Pedersen KO. Quasi-brittle fracture during structural impact of AA7075-T651 aluminium plates. International Journal of Impact Engineering 2010;37:537–51.

[27] Børvik T, Langseth M, Hopperstad OS, Malo KA. Ballistic penetration of steel plates. International Journal of Impact Engineering 1999;22:855–87.

[28] Børvik T, Forrestal MJ, Warren TL. Perforation of 5083-H116 aluminum armor plates with ogive-nose rods and 7.62mm APM2 bullets. Experimental Mechanics; 2009; doi:10.1007/s11340-009-9262-5.

[29] Forrestal MJ, Børvik T, Warren TL. Perforation of 7075-T651 aluminum armor plates with 7.62mm APM2 Bullets. Experimental Mechanics; 2009; doi:10.1007/s11340-009-9328-4.

[30] Mayers MA. Dynamic behavior of materials. New York: John Wiley & Sons; 1994.

[31] Hiermaier S. Structures under crash and impact. New York: Springer; 2008.

[32] Steinberg DJ. Equation of state and strength properties of selected materials. Report No. UCRL-MA-106439. Livermore, CA: Lawrence Livermore National Laboratory; 1991. 1–67.

[33] Lukyanov AA. Constitutive behaviour of anisotropic materials under shock loading. International Journal of Plasticity 2008;24:140–67.

[34] Zukas JA, et al. High velocity impact dynamics. New York: John Wiley & Sons; 1990.

[35] Børvik T, Dey S, Olovsson L, Langseth M. Impact of APM2 bullets on AA6082-T4 aluminium plates. In: F. Schäfer & S. Hiermaier (eds) Proceedings of the 11th hypervelocity impact symposium (p. 13), 11–15 April 2010, Freiburg, Germany.